

Spontaneous Symmetry Breaking in a Coherently Driven Nanophotonic Bose-Hubbard Dimer

B. Garbin¹, A. Giraldo^{2,3}, K. J. H. Peters⁴, N. G. R. Broderick^{5,3}, A. Spakman⁴, F. Raineri^{1,6},
A. Levenson¹, S. R. K. Rodriguez⁴, B. Krauskopf² and A. M. Yacomotti¹

¹Université Paris-Saclay, CNRS, Centre de Nanosciences et de Nanotechnologies, 91120 Palaiseau, France

²Department of Mathematics and Dodd-Walls Centre, The University of Auckland,
Private Bag 92019, Auckland 1142, New Zealand

³Photon Factory, Department of Physics, University of Auckland, Auckland 1010, New Zealand

⁴Center for Nanophotonics, AMOLF, Science Park 104, 1098 XG Amsterdam, Netherlands

⁵Department of Physics and Dodd-Walls Centre, The University of Auckland, Private Bag 92019, Auckland 1142, New Zealand

⁶Université Côte d'Azur, Institut de Physique de Nice, CNRS-UMR 7010, Sophia Antipolis, France



(Received 29 July 2021; accepted 13 December 2021; published 4 February 2022)

We report on the first experimental observation of spontaneous mirror symmetry breaking (SSB) in coherently driven-dissipative coupled optical cavities. SSB is observed as the breaking of the spatial or mirror \mathbb{Z}_2 symmetry between two symmetrically pumped and evanescently coupled photonic crystal nanocavities, and manifests itself as random intensity localization in one of the two cavities. We show that, in a system featuring repulsive boson interactions ($U > 0$), the observation of a pure pitchfork bifurcation requires negative photon hopping energies ($J < 0$), which we have realized in our photonic crystal molecule. SSB is observed over a wide range of the two-dimensional parameter space of driving intensity and detuning, where we also find a region that exhibits bistable symmetric behavior. Our results pave the way for the experimental study of limit cycles and deterministic chaos arising from SSB, as well as the study of nonclassical photon correlations close to SSB transitions.

DOI: [10.1103/PhysRevLett.128.053901](https://doi.org/10.1103/PhysRevLett.128.053901)

The Bose-Hubbard dimer (BHD) is a paradigmatic system featuring quantum dynamics of bosons hopping across sites and interacting on site [1]. The competition between these processes in the *closed* BHD unveiled a wealth of quantum and classical nonlinear phenomena, including self-trapping [2] and symmetry breaking [3]. In most real BHDs, however, particle losses need to be compensated by external driving [4–7]. These *driven-dissipative* BHDs have recently drawn much interest, as they display intriguing classical [8,9] and quantum [10] phenomena due to the balance between driving and dissipation. Driven-dissipative BHDs have been implemented on light-matter systems like semiconductor microcavities [11–13] and superconducting circuits [14,15].

Spontaneous symmetry breaking (SSB) is a universal phenomenon occurring when a symmetric system ends up in an asymmetric state. SSB and its applications have attracted significant interest in optics [16–23]. In single coherently driven optical cavities, SSB emerges from the nonlinear coupling between two polarization [24] or counterpropagating [21] modes [25–28]. SSB has also been observed in evanescently coupled photonic crystal nanolasers [19], which share some properties with incoherently driven BHDs [29]. However, optical gain saturation—a nonlinear mechanism reminiscent of inelastic two body collisions in atomic systems [8]—results in a

fundamental difference with respect to BHDs. Compared to the incoherent pumping case, coherent driving offers a more versatile parameter control and suppressed spontaneous emission noise. Furthermore, coherently driven BHD have been predicted to undergo entanglement close to the SSB transition [30], thereby bridging classical nonlinear dynamics and quantum optics.

Despite the strong interest in coherently driven dissipative BHD physics, SSB remains unreported. This is likely due to two reasons. First, conventional driven-dissipative BHDs display symmetry broken phases restricted to narrow parameter regions, which coexist with other optical bistabilities [9,31]. Thus, accessing SSB is challenging. Second, resonant optical excitation experiments require mode matching, thereby leading to more stringent conditions than their incoherent pumping counterparts.

Here we demonstrate coherently driven SSB in a photonic crystal driven-dissipative BHD. Unlike standard BHDs, our system features a negative photon hopping energy that, in conjunction with a positive on site interaction energy, results in a broken symmetry phase across large parameter regions [9]. These are *pure* pitchfork-bifurcated phases; they do not coexist with a bistable homogeneous state which might otherwise hinder the SSB observation.

We consider a BHD of two sites—“or cavities”—that is coherently driven symmetrically with amplitude F and

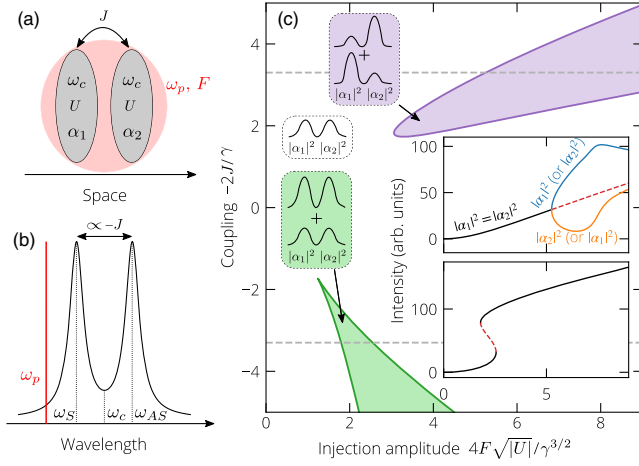


FIG. 1. Illustration of (a) two evanescently coupled injected resonators and (b) the resulting split hybrid symmetric (ω_S) and antisymmetric (ω_{AS}) modes. (c) Two-parameter bifurcation diagram for $\Delta = 0$ showing the regions of bistability of symmetric (green region) and asymmetric (purple region) steady states. The insets represent bifurcation slices showcasing the existence of pitchfork (top, $-2J/\gamma = +3.3$) and saddle-node (bottom, $-2J/\gamma = -3.3$) bifurcations.

frequency ω_p , where photons interact on site with energy $U > 0$ and hop across sites with energy $J < 0$ [see Fig. 1(a)]. Here, U and J respectively represent the nonlinearity per photon and the photon hopping rate [31]. We apply the truncated Wigner approximation [4], neglecting quantum correlations but accounting for quantum fluctuations via stochastic terms in semiclassical equations of motion. In a frame rotating at ω_p , the expectation values $\alpha_{1,2}$ of the bosonic operators \hat{a}_1 and \hat{a}_2 in the two sites satisfy

$$i \frac{d\alpha_{1,2}}{dt} = \left(-\Delta - i\frac{\gamma}{2} + 2U|\alpha_{1,2}|^2 \right) \alpha_{1,2} - J\alpha_{2,1} + F_{1,2} + \sqrt{\frac{\gamma}{2}} \zeta_{1,2}(t). \quad (1)$$

Here, $\Delta = \omega_p - \omega_c$ is the detuning between ω_p and the cavities' resonance frequency ω_c , and $F_1 = F_2 = F$ are the coherent driving amplitudes applied to each cavity, taken to be equal here γ is the loss rate. The last term in Eq. (1) models the fluctuations as complex Gaussian noise terms $\zeta_j(t) = [\zeta'_j(t) + i\zeta''_j(t)]/\sqrt{2}$ ($j = 1, 2$) which have zero mean and are delta-correlated in t .

In our experimental implementation, the sites are given by two evanescently coupled photonic crystal (PHC) nanocavities with embedded quantum wells (QWs) illuminated by an optically resonant laser field. The bosons are intracavity photons that experience carrier-induced dispersive nonlinearities for energies below the QW absorption maximum ($\lambda_{QW} \approx 1510$ nm), and carrier densities below QW-absorption saturation. Within our excitation range

($\lambda \sim 1565$ nm), band filling due to one photon absorption dominates, leading to a blueshifting intensity-dependent refractive index ($U > 0$) [32–35]. Using Eq. (1) to model the PHC dimer, we assume instantaneous Kerr nonlinearity due to ultrafast carrier dynamics.

For identical cavities with $2|J| > \gamma$ and in the linear regime, two hybrid modes arise [Fig. 1(b)]: the symmetric mode with $\alpha_1 = \alpha_2$, and the antisymmetric mode with $\alpha_1 = -\alpha_2$; the mode splitting and their relative spectral position, respectively, depend on the magnitude and sign of J . Upon coherent in-phase symmetric illumination of the two cavities, only the symmetric mode is excited. The sign of J has a large impact on the observed behavior [Fig. 1(c)]: provided $U > 0$, pure SSB only exists for $J < 0$ (purple region and top inset). For $J > 0$, the bistability of the homogeneous symmetric states prevails (green region and bottom inset); see Fig. 1(c) for $\Delta = 0$.

Decreasing the value of Δ from zero results in an overlap of these two regions near $J = 0$; this creates regions of, e.g., periodic and chaotic behavior (see Supplemental Material [36]). For $J > 0$, however, the SSB transition always lies inside the bistable symmetric zone. On the contrary, the pure supercritical pitchfork bifurcation is only warranted for $J < 0$, which we can implement experimentally.

Figure 2(a) shows our experimental setup. Two evanescently coupled photonic-crystal nanoresonators are realized as optical defects (three missing holes, known as L3 cavities) in a 2D triangular lattice of air holes in a

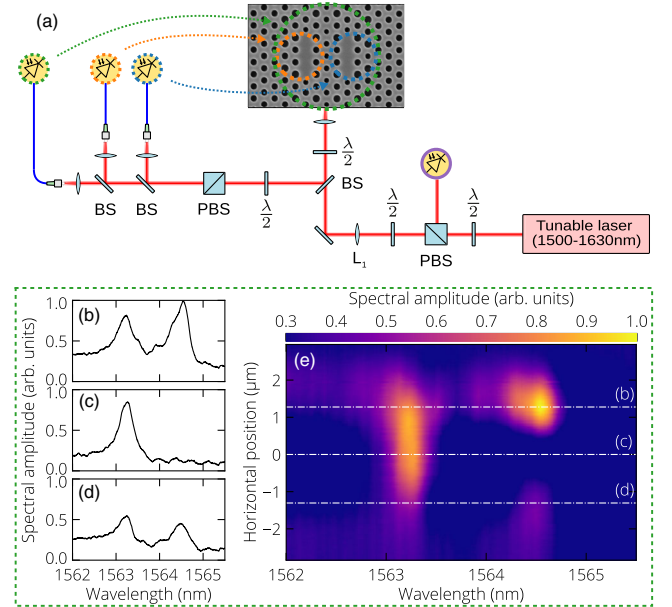


FIG. 2. Experimental setup and operational regime. (a) Schematic of the experimental setup. BS, beam splitter; PBS, polarizing beam splitter; L_1 , 100 cm focal lens; linear spectroscopy (dashed green circles) and individual cavity output (blue and orange dashed circles). (b)–(d) Selected spectra for given sample horizontal positions. (e) Evolution of the spectra with the sample horizontal position.

free-standing InP membrane. Photons are confined in the plane thanks to the photonic band gap. Furthermore, the nonlinearity is provided by confined charge carriers in four embedded $\text{In}_{0.53}\text{Ga}_{0.47}\text{As}$ QWs. The lattice period a is 435 nm (hole radii $r_0 = 116$ nm). Spatial mode matching of the illumination laser beam to the cavity mode is enhanced by means of far-field engineering of the PHC cavity [37] (hole radii $r_2 = 137$ nm). Such mode matching is further improved by using a lens with 100 cm focal length (L_1 in Fig. 2). Importantly, negative J is the consequence of a larger effective refractive index of the antisymmetric mode in the underlying two-coupled $W1$ waveguides. Targeted mode splitting is further achieved by modifying the radii of the central row of holes (hole radii $r_{0,2} - 20\%$) [19,37]. The two cavities are coherently driven close to their resonant wavelength (≈ 1563.9 nm) with a narrow-linewidth widely tunable laser, whose beam is split for injection power monitoring. Finally, a $100\times$ magnification with 0.95 numerical aperture microscope objective (Olympus MPLAN x100 IR) focuses the laser beam to a $2.2\ \mu\text{m}$ diameter spot on the sample from the top. The sample is mounted on a PZT driven 6-axis translation stage for controlling the relative position between the driving beam and the cavities and, hence, the relative power impinging on the two cavities. We use a half wave plate to rotate the linearly polarized injection beam at input, by 45° from the cavities' polarization. The cavities' outputs are subsequently separated from the reflected part of the injection beam with polarization optics, and split to allow spectral and temporal analysis. The spectral part is directed to a liquid-nitrogen-cooled spectrometer (Acton SP 2500). To independently analyze three different regions of the sample, the reflected intensity is split, selectively coupled into three different single mode fibers, and directed to (i) a 750 Hz bandwidth Newfocus fW detector for linear spectroscopy (large dashed circle in Fig. 2) and (ii) two 550 MHz bandwidth low-noise APD detectors (Princeton Lightwave PLA-8XX, $\text{NEP} = 250\ \text{fW}/\sqrt{\text{Hz}}$) for measuring the output intensity of each cavity (smaller dashed circles in Fig. 2).

We first perform linear reflectivity spectroscopy by sweeping the driving laser wavelength. Figures 2(b)–2(d) show spectra for selected horizontal positions of the driving beam, measured with the fw detector. The relative excitation of the two hybrid modes depends on the spatial location of the driving beam relative to the sample. For an off-centered beam [Figs. 2(b) and 2(d)] both modes are excited. For a centered beam [Fig. 2(c)], only the symmetric mode is excited. Figure 2(e) shows a collection of such spectra with the driving position varied along the horizontal axes. It allows us to identify the central driving condition (horizontal position labeled $0\ \mu\text{m}$) which minimizes driving asymmetries [$F_1 \approx F_2$; see Eq. (1)].

Since J is negative, the symmetric mode is located at a shorter wavelength (1563.2 nm) than the antisymmetric one

(1564.5 nm). Based on the measured mode splitting (1.3 nm) and mode linewidth (0.39 nm), we estimate the normalized coupling constant $\kappa = -2J/\gamma \approx 3.3$; this is compatible with SSB observation for low excitation power. Increasing the splitting to $|\kappa| \gtrsim 5$, for instance without barrier hole modification, increases the injection amplitude of the SSB threshold and might hinder observation [see Fig. 1(c)].

After locating the illumination spot at the center of the dimer [line (c) in Fig. 2(e)], the excitation power (purple traces in Fig. 3) is ramped up to about 1.5 mW within ~ 300 ns to minimize thermal effects. Figures 3(a) to 3(b) show typical cavity intensity time traces (blue and orange curves) for two different values of the normalized detuning $\delta = -2\Delta/\gamma$. At low driving powers, the two cavity output traces are coincident, indicating that a delocalized (symmetric) hybrid mode is being excited. At a time of about 285 ns, however, the two output intensities part, which we identify as the SSB transition point. The spontaneous character of the SSB manifests itself as randomly selected asymmetric states (Fig. 3, top and middle traces). The bottom traces in Fig. 3, built by overlapping maxima of histograms of 500 successive realizations, evidence the mirror symmetry of the two asymmetric states (see Supplemental Material [36] for comparisons with numerical simulations), and can be seen as the reconstruction of the underlying pitchfork bifurcation.

When increasing the magnitude of the detuning from Figs. 3(a) to 3(b), we need to realign the illumination spot to observe randomly selected asymmetric states. This may be understood from Eq. (1) in the presence of asymmetries in the cavity frequencies ($\omega_{c,1} \neq \omega_{c,2}$) and driving fields ($F_1 \neq F_2$). The first one is due to unavoidable fabrication imperfections ($\approx 0.13 \pm 0.07$ nm), while the second one accounts for deviations of the illumination spot from the dimer center. Indeed, numerical simulations (not shown) indicate that the asymmetry parameter $\xi \sim F_1 - F_2$ that

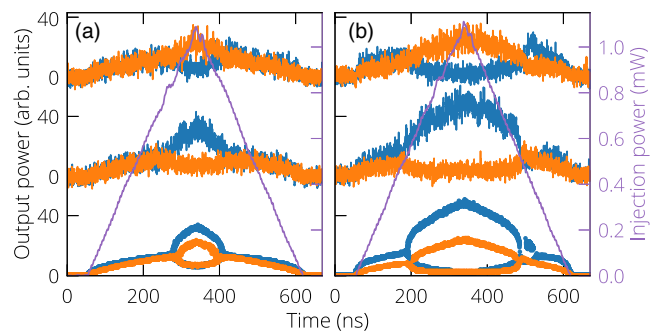


FIG. 3. Temporal observation of SSB. (a),(b) Top and middle traces are subsequent realizations of the same experiment. Bottom traces are histogram maxima computed from 500 realizations; shown are the output powers of the two cavities (blue and orange, respectively) and the driving power (purple curve). (a) $\delta = -1.59$. (b) $\delta = -2.86$.

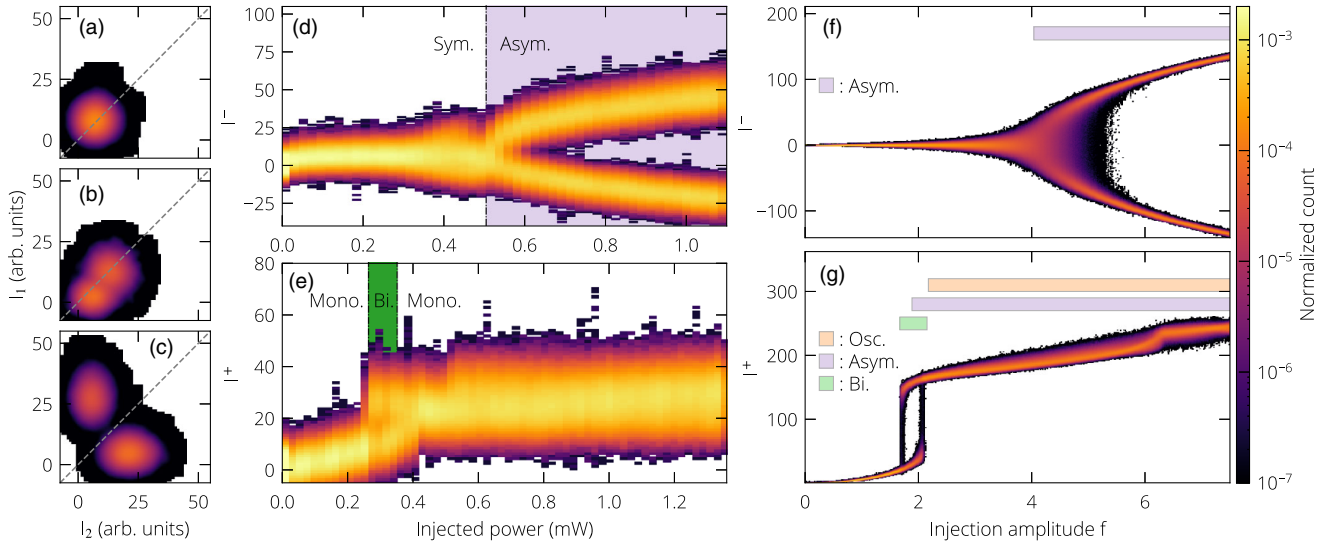


FIG. 4. Identification of operational regimes. (a)–(c) Selected projections of the phase space showing monostable symmetric, bistable symmetric, and bistable asymmetric steady states, respectively. (d),(e) Experimental and (f),(g) numerical histograms computed from 500 realizations, showing I^- [(d),(f)] and I^+ [(e),(g)] versus injection strength. (a) 0.22 mW. (b) 0.26 mW. (c) 1.03 mW. (a),(c) $\delta = -0.82$. (d),(f) $\delta = -2.86$. (b),(e),(g) $\delta = -6.19$.

induces random switching changes with Δ , consistent with the experimental observation; this explains the difference in cavity intensities (blue and orange curves) when moving from Figs. 3(a) to 3(b) related to slight misalignment in the optical detection devices. The observation of SSB through compensation of two asymmetry parameters has recently been reported in Ref. [24].

Notice further that Fig. 3(b) also shows an asymmetry when comparing the ramping up and down measurement. We attribute this to either or both (i) small asymmetries in the cavities' design that influences the position of the transitions and (ii) a critical slowing down at the SSB transition induced by the ramp [38].

Figure 4 illustrates the three main regimes of operation observed in our experiment, as well as the associated SSB transition and bistability. Projections of the phase space onto the (I_1, I_2) plane of the two measured intensities, for given values of injection power and detuning, show (i) equal intensity in the two cavities [Fig. 4(a)], (ii) bistable operation with symmetric cavity intensities [Fig. 4(b)], and (iii) bistable operation with asymmetric cavity intensities [symmetry broken states, Fig. 4(c)]. To identify the different phases and transitions as parameters change, we consider the intensity difference $I^- = I_1 - I_2$ and sum $I^+ = I_1 + I_2$, which indicate the presence of asymmetric and symmetric states by highlighting anticorrelations and correlations, respectively (see Supplemental Material [36]). To identify the number of states as the injected power is varied, we analyze, for two given values of detuning, the number of maxima in I^- and I^+ [Figs. 4(d) and 4(e), respectively]. For comparatively small detunings as in Fig. 4(d), I^- exhibits, at an injected power of about

0.51 mW, a SSB transition from a single to two asymmetric coexisting steady states [see Fig. 4(c)]. For comparatively large detunings as in Fig. 4(e), on the other hand, I^+ exhibits two maxima in the range of injected power from 0.26 mW to 0.35 mW, which is evidence for a region of bistability with two coexisting symmetric steady states [see Fig. 4(b)].

Figures 4(f) and 4(g) show corresponding plots obtained by simulating Eq. (1) while varying the normalized driving amplitude $f = 4F\sqrt{|U|}/\gamma^{3/2}$. We also set $U = \gamma/100$, which we estimated by comparing numerical and experimental standard deviations of the intensity around the SSB transition. Further rescaling the intracavity field as $(A, B) = (-2i\alpha_1^*\sqrt{|U|/\gamma}, -2i\alpha_2^*\sqrt{|U|/\gamma})$ [9] allows us to interpret $\gamma/|U| \sim 100$ as the characteristic intracavity photon number; note that the thermodynamic limit corresponds to $\gamma/|U| \rightarrow \infty$, for which the mean-field solutions—i.e., those without stochastic fluctuations—are strictly justified. Analytical results of bifurcation points of the mean-field BHD derived in [9] give an important handle to analyse the stochastic simulation results. Firstly, the mean-field pitchfork bifurcation associated with the SSB transition occurs at $f \approx 4.04$ in Fig. 4(f); this is consistent with the stochastic numerical simulations, which also indicate the presence of random switching between asymmetric states from this value up to $f \approx 5.5$. Secondly, the two predicted mean-field bifurcations of the symmetric state for $1.67 \lesssim f \lesssim 2.15$ clearly set the limits of the observed hysteresis cycle in Fig. 4(g).

We now identify in Fig. 5 the different regimes of operation in the two-dimensional parameter plane of

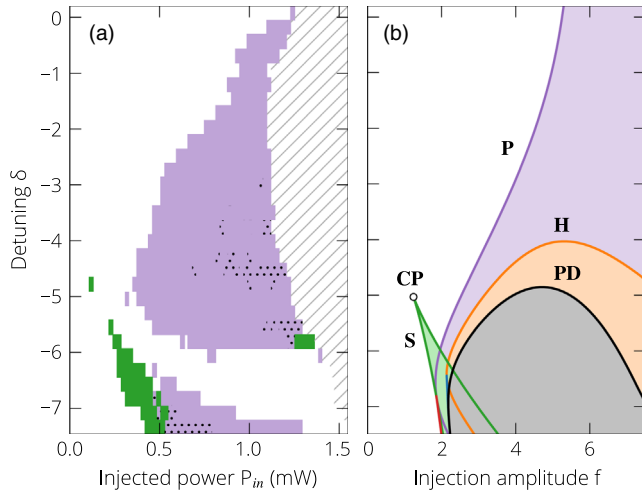


FIG. 5. Two-parameter bifurcation diagrams in injection strength and detuning. (a) Experimental; colors stand for the number of maxima observed: white, one maximum for both I^+ and I^- ; purple, two maxima for I^- ; green, two maxima for I^+ ; dotted area, superposition of green and purple; hatched area, not investigated. (b) Numerical; curves represent different bifurcations: purple, pitchfork; green, saddle-node of symmetric steady states; orange, Hopf; black, period doubling; shades of purple, regions with asymmetric solutions.

driving strength and detuning. The experimental bifurcation diagram in Fig. 5(a) was created by color coding the number of maxima found for I^+ and I^- . It reveals large regions of the parameter plane for which the system exhibits two asymmetric steady states; the SSB transition that bounds this region to the left moves toward lower injection power P_{in} as the detuning δ is decreased; it is characterized by distinct maxima of I^- . Notice also the region of symmetric bistability (identified by maxima of I^+ only) that exists for smaller δ ; it may also overlap (dotted area) with asymmetric behavior: three states are observed (one lower symmetric and two higher asymmetric). We attribute the absence of asymmetric states for $-7 \lesssim \delta \lesssim -6$ to large deviations of the sample's position with regard to the laser beam at larger detunings.

Figure 5(b) shows the associated two-parameter bifurcation diagram of Eq. (1) without noise (see Supplemental Material [36]) computed with AUTO07P [39]. Overall, it is in good agreement with the experimental bifurcation diagram in terms of where symmetry-broken dynamics and bistability between symmetric states can be found. More specifically, the saddle-node bifurcation curve **S** with the cusp point **CP** at $(f, \delta) \approx (1.24, -5.03)$ delimits the region with bistability between symmetric steady states. The SSB transition is identified as a pitchfork bifurcation **P** [30,31], yielding a region with two coexisting asymmetric steady states. As the detuning is decreased, the Hopf bifurcation curve **H** marks the onset of asymmetric oscillations, whereas **PD** indicates the first bifurcation of a period-doubling route to chaos, which eventually creates a pair of asymmetric

chaotic attractors that are each confined to one cavity [9]; they eventually collide, forming a symmetric chaotic attractor that features irregular switching between the two cavities [40]. This irregular switching has recently been observed in microresonators [41].

In conclusion, we have reported the first experimental realization of SSB in a coherently driven photonic dimer. For repulsive nonlinearities ($U > 0$), we have shown that pure supercritical pitchfork bifurcations only exist for negative photon hopping energies ($J < 0$); we also predict this to hold for $J > 0$ provided that $U < 0$. The SSB transition consists of the splitting of the two intracavity intensities under symmetric driving conditions; this is observed as two different randomly selected states where light is localized in either of the two cavities. We mapped out the SSB transition in a large parameter plane and identified the region of bistability between symmetric states. Our experiments are in good agreement with the mean-field Bose-Hubbard dimer model, and stochastic simulations validated the random nature of this process. The theory for the BHD also predicts the existence of limit cycle oscillations and deterministic chaos. Our results constitute an important step toward the study of symmetry breaking in the few photon regime [30], at the crossroad between nonlinear dynamics and quantum optics.

We thank I. Sagnes for discussions. B. G. and A. M. Y. would like to acknowledge the financial support from the European Union in the form of Marie Skłodowska-Curie Action Grant No. MSCA-841351. This work is supported by a public grant overseen by the French National Research Agency (ANR) as part of the ‘‘Investissements d’Avenir’’ program (Labex NanoSaclay, reference: ANR-10-LABX-0035) and by the ANR UNIQ DSO78. This work is part of the research program of the Netherlands Organisation for Scientific Research (NWO). S. R. K. R. acknowledges an ERC Starting Grant with Project No. 85269.

-
- [1] M. P. A. Fisher, P. B. Weichman, G. Grinstein, and D. S. Fisher, *Phys. Rev. B* **40**, 546 (1989).
 - [2] M. Albiez, R. Gati, J. Fölling, S. Hunsmann, M. Cristiani, and M. K. Oberthaler, *Phys. Rev. Lett.* **95**, 010402 (2005).
 - [3] T. Zibold, E. Nicklas, C. Gross, and M. K. Oberthaler, *Phys. Rev. Lett.* **105**, 204101 (2010).
 - [4] I. Carusotto and C. Ciuti, *Rev. Mod. Phys.* **85**, 299 (2013).
 - [5] S. Schmidt and J. Koch, *Ann. Phys. (Berlin)* **525**, 395 (2013).
 - [6] M. J. Hartmann, *J. Opt.* **18**, 104005 (2016).
 - [7] C. Noh and D. G. Angelakis, *Rep. Prog. Phys.* **80**, 016401 (2016).
 - [8] P. Coulet and N. Vandenberghe, *Phys. Rev. E* **64**, 025202(R) (2001).
 - [9] A. Giraldo, B. Krauskopf, N. G. R. Broderick, J. A. Levenson, and A. M. Yacomotti, *New J. Phys.* **22**, 043009 (2020).
 - [10] F. Minganti, A. Biella, N. Bartolo, and C. Ciuti, *Phys. Rev. A* **98**, 042118 (2018).

- [11] K. G. Lagoudakis, B. Pietka, M. Wouters, R. André, and B. Deveaud-Plédran, *Phys. Rev. Lett.* **105**, 120403 (2010).
- [12] M. Abbarchi, A. Amo, V. G. Sala, D. D. Solnyshkov, H. Flayac, L. Ferrier, I. Sagnes, E. Galopin, A. Lemaître, G. Malpuech *et al.*, *Nat. Phys.* **9**, 275 (2013).
- [13] S. R. K. Rodriguez, A. Amo, I. Sagnes, L. Le Gratiet, E. Galopin, A. Lemaître, and J. Bloch, *Nat. Commun.* **7**, 11887 (2016).
- [14] J. Raftery, D. Sadri, S. Schmidt, H. E. Türeci, and A. A. Houck, *Phys. Rev. X* **4**, 031043 (2014).
- [15] C. Eichler, Y. Salathe, J. Mlynek, S. Schmidt, and A. Wallraff, *Phys. Rev. Lett.* **113**, 110502 (2014).
- [16] A. E. Kaplan and P. Meystre, *Opt. Lett.* **6**, 590 (1981).
- [17] *Spontaneous Symmetry Breaking, Self-Trapping, and Josephson Oscillations*, edited by B. A. Malomed (Springer, Berlin, 2013).
- [18] M. Liu, D. A. Powell, I. V. Shadrivov, M. Lapine, and Y. S. Kivshar, *Nat. Commun.* **5**, 4441 (2014).
- [19] P. Hamel, S. Haddadi, F. Raineri, P. Monnier, G. Beaudoin, I. Sagnes, A. Levenson, and A. M. Yacomotti, *Nat. Photonics* **9**, 311 (2015).
- [20] Q.-T. Cao, H. Wang, C.-H. Dong, H. Jing, R.-S. Liu, X. Chen, L. Ge, Q. Gong, and Y.-F. Xiao, *Phys. Rev. Lett.* **118**, 033901 (2017).
- [21] L. Del Bino, J. M. Silver, S. L. Stebbings, and P. Del’Haye, *Sci. Rep.* **7**, 43142 (2017).
- [22] G. Xu, A. U. Nielsen, B. Garbin, L. Hill, G.-L. Oppo, J. Fatome, S. G. Murdoch, S. Coen, and M. Erkintalo, *Nat. Commun.* **12**, 4023 (2021).
- [23] N. Moroney, L. Del Bino, S. Zhang, M. T. M. Woodley, L. Hill, T. Wildi, V. J. Wittwer, T. Südmeyer, G.-L. Oppo, M. R. Vanner, V. Brasch, T. Herr, and P. Del’Haye, *arXiv*: 2104.13892.
- [24] B. Garbin, J. Fatome, G.-L. Oppo, M. Erkintalo, S. G. Murdoch, and S. Coen, *Phys. Rev. Research* **2**, 023244 (2020).
- [25] M. Haelterman, S. Trillo, and S. Wabnitz, *J. Opt. Soc. Am. B* **11**, 446 (1994).
- [26] J. Geddes, J. Moloney, E. Wright, and W. Firth, *Opt. Commun.* **111**, 623 (1994).
- [27] M. T. M. Woodley, J. M. Silver, L. Hill, F. Copie, L. Del Bino, S. Zhang, G.-L. Oppo, and P. Del’Haye, *Phys. Rev. A* **98**, 053863 (2018).
- [28] L. Hill, G.-L. Oppo, M. T. M. Woodley, and P. Del’Haye, *Phys. Rev. A* **101**, 013823 (2020).
- [29] M. Seclì, M. Capone, and M. Schirò, *New J. Phys.* **23**, 063056 (2021).
- [30] W. Casteels and C. Ciuti, *Phys. Rev. A* **95**, 013812 (2017).
- [31] B. Cao, K. W. Mahmud, and M. Hafezi, *Phys. Rev. A* **94**, 063805 (2016).
- [32] S. W. Koch, N. Peyghambarian, and H. M. Gibbs, *J. Appl. Phys.* **63**, R1 (1988).
- [33] M. Sheik-Bahae, D. J. Hagan, and E. W. Van Stryland, *Phys. Rev. Lett.* **65**, 96 (1990).
- [34] J. Mondia, H. Tan, S. Linden, H. van Driel, and J. Young, *J. Opt. Soc. Am. B* **22**, 2480 (2005).
- [35] K. Nozaki, T. Tanabe, A. Shinya, S. Matsuo, T. Sato, H. Taniyama, and M. Notomi, *Nat. Photonics* **4**, 477 (2010).
- [36] See Supplemental Material at <http://link.aps.org/supplemental/10.1103/PhysRevLett.128.053901> for the numerical observation of SSB in the presence of noise, the identification of bistability of symmetric and asymmetric states, and the observation of pure SSB in the normalized model without noise.
- [37] S. Haddadi, P. Hamel, G. Beaudoin, I. Sagnes, C. Sauvan, P. Lalanne, J. A. Levenson, and A. M. Yacomotti, *Opt. Express* **22**, 12359 (2014).
- [38] J. R. Tredicce, G. L. Lippi, P. Mandel, B. Charasse, A. Chevalier, and B. Picqué, *Am. J. Phys.* **72**, 799 (2004).
- [39] E. J. Doedel, B. E. Oldeman, A. R. Champneys, F. Dercole, T. F. Fairgrieve, Y. A. Kuznetsov, R. C. Paffenroth, B. Sandstede, X. Wang, and C. Zhang, AUTO-07P software (2012).
- [40] A. Giraldo, N. G. R. Broderick, and B. Krauskopf, *Discrete Contin. Dyn. Syst. Ser. B*, Online First (2021).
- [41] M. T. M. Woodley, L. Hill, L. Del Bino, G.-L. Oppo, and P. Del’Haye, *Phys. Rev. Lett.* **126**, 043901 (2021).